Table of contents

S1. Areal capacity values of synthesized electrodes

Table S1. Areal capacity values of synthesized electrodes.

Sample	Areal capacity (mAh/cm²)
Bare Ni	0.011
Fe	0.016
$Fe_{0.75}V_{0.25}$	0.091
$Fe_{0.5}V_{0.5}$	0.058
$Fe_{0.25}V_{0.75}$	0.045
V	0.025

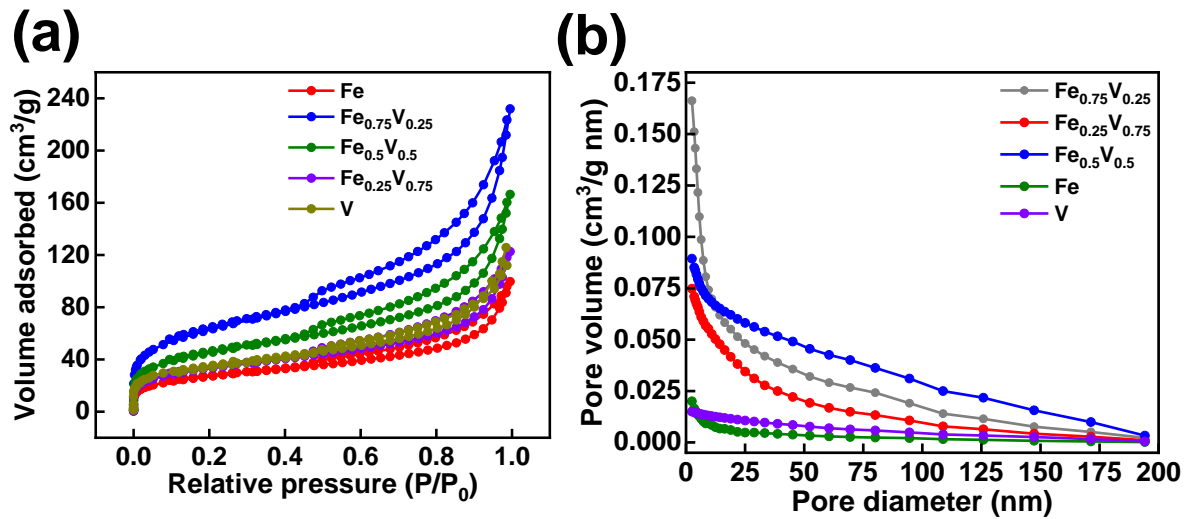**S2. BET and BJH study of all the electroactive materials.**

Figure S1. (a) Brunauer-Emmett-Teller (BET) nitrogen adsorption-desorption isotherm and (b) Barrett-Joyner-Halenda (BJH) pore size distribution curve of all the electroactive materials (i.e., Fe, $Fe_{0.75}V_{0.25}$, $Fe_{0.5}V_{0.5}$, and $Fe_{0.25}V_{0.75}$, and V).

S3. Surface area and pore size of synthesized samples.

Table S2. Surface area and pore size of synthesized samples.

Sample	Surface area (m²/g)	Pore size (nm)
Fe	21.55	12.07
$Fe_{0.75}V_{0.25}$	98.63	1.48
$Fe_{0.5}V_{0.5}$	63.21	5.53
$Fe_{0.25}V_{0.75}$	44.58	6.52
V	36.21	9.78

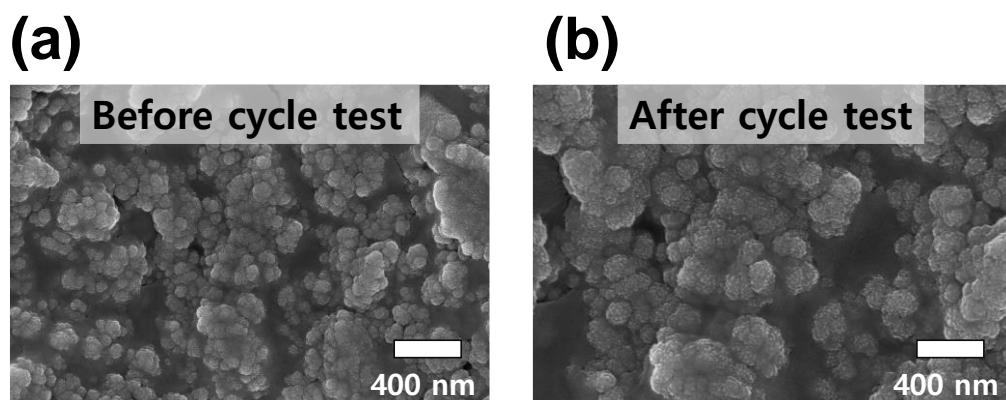**S4. SEM analysis of FeV-LDH before and after cycling stability study.**

Figure S2. SEM images of FeV LDH electrode (a) before GCD cycle stability study, (b) after 5,000 GCD cycles at 20 mA/cm².

S5. Preparation and electrochemical performance of AC//SP negative electrode.

Deposition of activated carbon on sand paper (AC//SP) was carried out using a simple slurry coating method. The active material (AC), super P carbon, and PVDF binder were reserved in a weight ratio of 80:10:10 and mixed thoroughly using an agate mortar with the help of few drops of N-methyl 2-Pyrrolidone (NMP) solvent till the thick uniform slurry formation. Then the slurry was distributed on sand paper substrate (1x1 cm²) followed by vacuum drying at 80 ℃ for 4 h. Electrochemical properties of AC//SP negative electrode were explored with the aid of cyclic voltammetry (CV), galvanostatic charge/discharge (GCD) in 1 M KOH electrolyte using an Iviumstat electrochemical workstation (IVIUM Technologies). CV plots were recorded at various sweep rates ranging from 10 to 50 mV/s within a potential window of -1 to 0 V. As explained from Figure S1a, the CV plots are in quasi-rectangle shapes, signifying the capacitive behavior of the electrode. Similar behavior is detected in GCD plots of the electrode recorded at different current densities varying from 3 mA/cm² to 10 mA/cm² (Figure S1b) with triangular shaped curves.
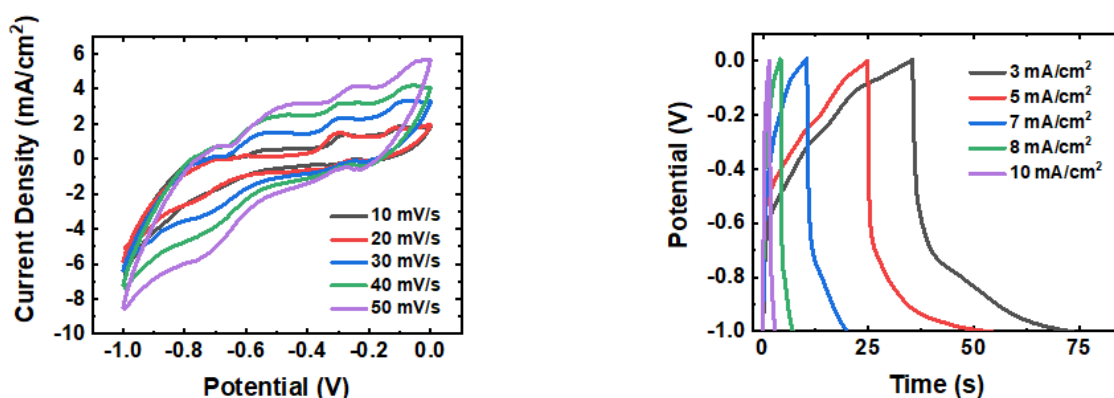

Figure S3. (a) CV curves of AC//SP electrode at different sweep rates varying from 10 to 50 mV/s, and (b) GCD curves of AC//SP electrode at various current densities ranging from 3 to 10 mA/cm².

S6. Comparison of the obtained HSC device energy storage properties with the previously reported HSC/asymmetric device performances.

Table S3. Comparison of the obtained HSC device energy storage properties with the previously reported HSC/asymmetric device performances.

References	Substrate	Electrolyte	Active material	Energy density	Power density
Ref [38]	Ni foam	2M KOH	MnFe	44.9 μW h/cm^2	16 mW/cm^2
Ref [39]	Ni foam	2M KOH	ZnCo	0.22 mW/cm^2	9 mW/cm^2
Ref [40]	Ni foam	2M KOH	NiAl	0.22 mWh/cm^2	4.5 mW/cm^2
Ref [41]	Ni foam	2M KOH	Ag	0.569 mWh/cm^2	3.82 mW/cm^2
Ref [42]	Ni foam	3M KOH	Co$_2$Al	0.102 mWh/cm^2	0.75 mW/cm^2
Our study	Sand paper	1M KOH	Fe$_{0.75}$V$_{0.25}$	0.123 mWh/cm^2	23.8 mW/cm^2

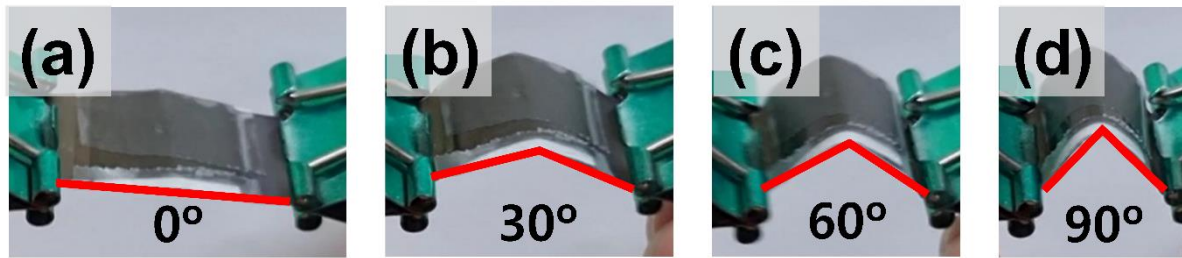**S7. Optical images of HSC device at different bending positions.**

Figure S4. Optical image of the HSC at flat and bending states and the definition of bending angle. (a) flat state, bending angle (b) 30º, (c) 60º, and (d) 90º.